electronics

MDPI

Article

Improved Repetitive Control for an LCL-Type Grid-Tied Inverter with Frequency Adaptive Capability in Microgrids

Hongwei Zhang [1], Qiangsong Zhao [1,*], Shuanghong Wang [1] and Xuebin Yue [2]

[1] School of Electronic and Information, Zhongyuan University of Technology, Zhengzhou 451191, China; zhanghongwei@zut.edu.cn (H.Z.)
[2] Department of Electronic and Computer Engineering, Ritsumeikan University, Kusatsu 525-8577, Japan
* Correspondence: zhaoqiangsong@zut.edu.cn

Abstract: Repetitive control (RC), which can track any periodic signal with a known integer period with zero steady-state error, is widely used for current control of grid-tied inverters in microgrids. However, the inherent one fundamental period time delay, leads to poor dynamic performance. Furthermore, the performance of conventional RC (CRC) will degrade when operating at a high variation grid frequency. Therefore, this paper proposes a frequency adaptive improved RC (FA-IRC) for grid-tied inverters. The improved RC (IRC) consists of a repetitive controller with a modified internal model filter, plus a proportional controller. In comparison to the CRC, the IRC has a good dynamic response, because it provides a higher gain and a wider bandwidth at the resonant frequency. Moreover, to achieve the frequency adaptability of the IRC, a fractional delay, based on a finite impulse response (FIR) filter, is built into the IRC system, to ensure that the resonant frequency of the IRC is approximately equal to the actual grid frequency and harmonic frequency. Stability analysis and characteristic analysis of the FA-IRC system are reported in this paper. Simulations are conducted, to demonstrate the validity of the proposed method.

Keywords: repetitive control; grid-tied inverter; FIR filter

check for updates

Citation: Zhang, H.; Zhao, Q.; Wang, S.; Yue, X. Improved Repetitive Control for an LCL-Type Grid-Tied Inverter with Frequency Adaptive Capability in Microgrids. *Electronics* **2023**, *12*, 1736. https://doi.org/10.3390/electronics12071736

Academic Editors: Da Xie, Yanchi Zhang, Dongdong Li, Chenghong Gu, Ignacio Hernando-Gil and Nan Zhao

Received: 1 March 2023
Revised: 3 April 2023
Accepted: 3 April 2023
Published: 5 April 2023

1. Introduction

Distributed power generation technologies using intermittent renewable energy sources, are an important means of solving energy problems and have therefore received extensive research [1,2]. As an important hub for energy conversion, the grid-tied inverter in the microgrid directly affects the stable and safe operation of the entire electrical energy system. Therefore, research on current harmonic suppression strategies for grid-tied inverters has received considerable attention [3].

Repetitive control (RC), based on the internal model principle (IMP), is widely used in inverter control, due to its advantage of high control accuracy, and it is particularly good at suppressing periodic disturbances, such as dead zones and periodic distortions in the output waveform, caused by non-linear rectifier loads or grid harmonics [4–7]. However, it has one fundamental period time delay. Furthermore, a repetitive controller can be equivalent to the sum of a negatively scaled term, an integral term, and a set of resonant controllers [8]. However, the negative proportional term will result in a slow transient response. To this end, researchers have proposed two methods to enhance the dynamic response of RC systems, one is to enable the system to have a higher RC gain and to increase the error convergence rate, by applying accurate phase compensation to the RC [9,10]. The other is to combine RC with a feedback control with fast dynamic response, typically in cascade or parallel, with a proportional or proportional-integral control, to form a composite control [11,12]. In [12], a proportional integral multi resonant-type RC (PIMR-RC), combining a repetitive controller and a proportional item, was proposed for control of grid-tied inverters, to enhance the transient response. This method has the benefit of a clearer design concept and improved low-frequency harmonic suppression performance.

The digital representation of the CRC is given by the formula $G_{CRC} = Q(z)z^{-N}/(1 - Q(z)z^{-N})$, where N is the order of RC and represents the proportion of the sampling frequency to the fundamental frequency. $Q(z)$ is typically a constant less than 1 or a zero-phase low-pass filter, to ensure a safe stability margin. In [13], a robust RC, based on a modified $Q(z)$ filter, was proposed, to obtain the performance improvement at the fundamental frequency. By utilizing this approach, it is possible to achieve a higher gain and a wider control bandwidth at the fundamental frequency, without the need for extensive computational resources. The wider bandwidth, implies that grid frequency variation in a small range (such as ± 0.2 Hz) does not significantly impact performance, which is suitable for control of the active power filter [14].

However, the N value in RC is usually rounded up or down when the grid frequency varies in a large range in distributed power generation systems. Consequently, the control gain of each harmonic will decline as the resonant frequency of the RC deviates from harmonic frequencies, resulting in harmonic suppression performance degrading and the total harmonic distortion (THD) increasing.

There are four main methods used to improve the frequency adaptation of RC: variable sampling frequency RC [15,16], bandwidth RC [17,18], higher-order RC (HORC) [19], and fractional-order RC (FORC) [20–23]. A scheme proposed in [15] ensures an integer RC order by changing the sampling rate, but real time changing of the sampling frequency increases the complexity of the controller implementation. In [16], a spatial RC based on the phase angle information of the grid voltage was proposed, which enables a guaranteed constant number of samples per cycle. It achieves a fixed number of samples per cycle, but the price paid is the inherent problem with the variable sampling method. Ref. [18] proposed a multi-bandwidth RC to resist the grid frequency variation in a grid-tied inverter. It sets each resonant bandwidth individually, and is implemented as a linear phase finite impulse response (FIR) filter, but the realization of the internal model filter is still complex. Using the HORC system, multi-cycle errors are accumulated. Compared to CRC, HORC can reduce interference at intermediate frequencies or against changes in the frequency of periodic signals [24]. However, on the other hand, this makes the system design more complex and computationally burdensome.

For frequency adaptability of the RC, the fractional-order RC (FORC) has been presented in many studies, which uses the fractional delay (FD) filter to approach the fractional order. The FORC with fractional delay Lagrange-interpolation-based FIR filter, has been proposed in a variety of applications [25–27]. In addition, in [28], a Thiran infinite impulse response (IIR) filter was proposed, to approximate the FD to enhance the frequency adaptability of CRC. Generally, the IIR filter has a full amplitude gain of one and requires only phase design, but it has poles, and the overall stability must be considered when designing the system, whereas with the FIR filter, stability issues do not need to be considered and it can be used directly. Nevertheless, the above fractional-order repetitive control using the FIR filter is CRC-based.

Therefore, this paper proposes a frequency adaptive improved RC (FA-IRC), to enhance the performance of a grid-tied inverter at grid frequency fluctuations. The control strategy is based on a novel improved repetitive control. The proposed IRC effectively increases the RC gain and resonance bandwidth at frequencies of interest, by introducing a positive proportional gain and a modified internal model filter repetitive controller, which speeds up the dynamic response time. Moreover, to further improve the frequency adaptation capability, the Lagrange interpolating-polynomial-based FIR filter is used to approximate the fractional part of the order of the IRC. Therefore, the proposed FA-IRC not only offers better dynamic performance, but also a lower THD when the grid frequency fluctuates.

The remainder of this article is organized as follows. An LCL-type grid-tied inverter system is introduced in Section 2. In Section 3, characteristics of the CRC, the PIMR-RC, and the proposed IRC are demonstrated. In Section 4, the FA-IRC with the FIR filter is established. The realization of fractional delay using an FIR filter is given. Moreover, a stability analysis and characteristic analysis of the FA-IRC system are performed. Section 5

discusses the simulation results that demonstrate the theoretical analysis's validity. Finally, conclusions are drawn in Section 6.

2. Grid-Tied Inverter System Modeling

Grid-tied inverters are widely used in microgrid distributed power generation systems. To prevent excessive harmonics, some filter topologies are proposed for grid-tied inverters. LCL filters have been used in place of L filters, to smooth the injected current with higher attenuation and reduction in size and weight of the components [29,30]. The impedance of the LLCL filter is almost zero at the switching frequency and therefore attenuates harmonic currents around the switching frequency [31]. The LLCL filter configuration simplifies the current control structure into single-loop current control, without extra damping loops. Nevertheless, extra control techniques are required to achieve active harmonic elimination.

Figure 1 shows an LCL-type single-phase grid-tied inverter control system [20]. In fact, the stability of a grid-tied inverter depends on the ratio of the grid impedance to the inverter impedance [32]. The stability of the internal current control loop of the individual inverter itself, in this paper, is related to the inherent LCL-filter resonance peak. To suppress the resonance peak of the LCL filter, a passive damping resistance R_d is employed. In Figure 1, PWM is an acronym for pulse width modulation, which is a commonly used control technique in power electronics, automatic control, and communication fields. It adjusts the width of the control signal's pulse, to control circuits or devices. ZOH stands for zero-order holder, which is a method for converting analog signals to digital signals. The phase-locked loop (PLL) is used to generate a signal whose phase is locked to the phase of the grid voltage at the point of common coupling (PCC). u_{inv} represents the output voltage of the inverter bridge, L_g represents the grid equivalent inductance, i_{ref} represents the tracked reference current, i_g represents the grid current, and u_g represents the grid voltage.

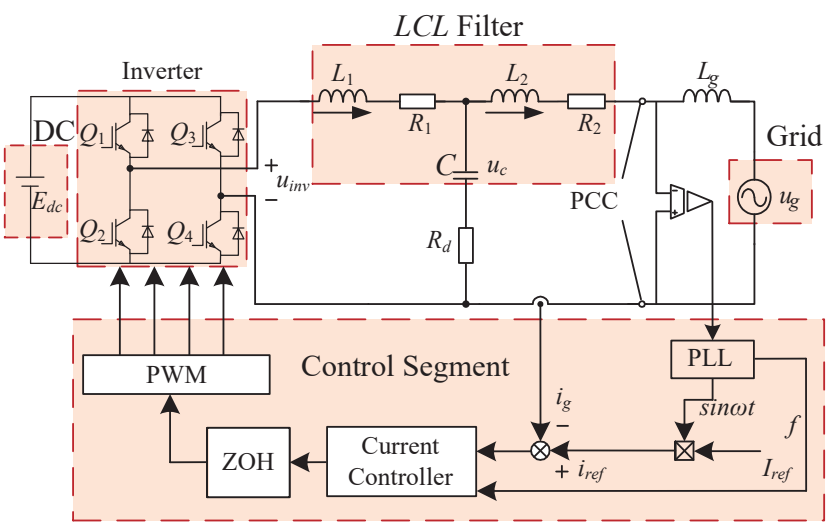

Figure 1. Model structure diagram of a single-phase LCL-type grid-tied inverter.

The equivalent resistance is ignored, and the transfer function from the input voltage u_{inv} to the grid current i_g is

$$G_{LCL}(s) = \frac{1 + R_d C s}{L_1 L_2 C s^3 + (L_1 + L_2) R_d C s^2 + (L_1 + L_2) s}. \quad (1)$$

The plant consists of a combination of inverter switches and the LCL filter, where the gain of the inverter switches is considered to be unity and the phase as zero degrees.

Therefore, the LCL filter is considered as the plant. The system parameters are given in Table 1. According to Table 1 and (1), it can be written in discretization as

$$P(z) = \frac{0.006802z^2 + 0.004736z - 0.002647}{z^3 - 1.991z^2 + 1.472z - 0.4803}. \tag{2}$$

Table 1. System parameters.

Parameters	Symbols	Value	Parameters	Symbols	Value
DC-link voltage	E_{dc}	380 V	L_1 equivalent resistance	R_1	0.48 Ω
Fundamental frequency	f_g	50 Hz	Grid-side inductor	L_2	2.5 mH
Sampling frequency	f_s	10 kHz	L_2 equivalent resistance	R_2	0.32 Ω
Switching frequency	f_{sw}	10 kHz	Output filter capacitance	C	10 μF
Inverter-side inductor	L_1	3 mH	Passive damping resistor	R_d	10 Ω
RMS value of grid voltage	u_g	220 V	Switching dead time	-	3 μs

3. Improved RC

3.1. CRC

The block diagram of CRC is shown in Figure 2, it can be written as:

$$G_{CRC}(z) = \frac{Q(z)z^{-N}}{1 - Q(z)z^{-N}}. \tag{3}$$

where $Q(z)$ and N are terms used in digital signal processing, with $Q(z)$ being an internal filter or a constant, and N representing the number of samples taken per cycle, with respect to the sampling frequency f_s and the grid fundamental frequency f_g. The transfer function of CRC in (3), can be derived as follows in the s-domain [8]:

$$\begin{aligned} G_{CRC}(s) = \frac{Qe^{-sT_0}}{1 - Qe^{-sT_0}} &= -\frac{1}{2} + \frac{1}{T_0 s + T_0\omega_c} + \frac{2}{T_0}\sum_{n=1}^{\infty} \frac{s + \omega_c}{s^2 + 2\omega_c s + \omega_c^2 + \left(\frac{2\pi n}{T_0}\right)^2} \\ &\approx -\frac{1}{2} + \frac{1}{T_0 s + T_0\omega_c} + \frac{2}{T_0}\sum_{n=1}^{\infty} \frac{s}{s^2 + 2\omega_c s + (n\omega_0)^2}, \end{aligned} \tag{4}$$

where $T_0 = 1/f_g = 2\pi/\omega_0$ is the fundamental period of the reference signal, ω_0 is the fundamental angular frequency, ω_c is the resonant bandwidth, and $\omega_c = -\ln Q/T_0$. It is clearly possible to see that the amplitude of $G_{CRC}(z)$ is nearly infinite at angular frequency $n\omega_0$, indicating that CRC can achieve zero steady-state error tracking for periodic signals.

However, it can be seen from Figure 2 and (3), that the internal mode of CRC can be decomposed into a positive feedback link and a delayed link. The former is used to accumulate signal, which acts as an integrator for periodic signals. The latter, however, is used to delay the output of the signal by one cycle, leading to a deteriorating influence on system performance. Moreover, the equivalent negative proportional term in (4), will result in a slow transient response. Hence, a PIMR-RC with CRC combined with a proportional gain, is proposed, in order to address this issue. The block diagram of the PIMR-RC system is shown in Figure 3 [12].

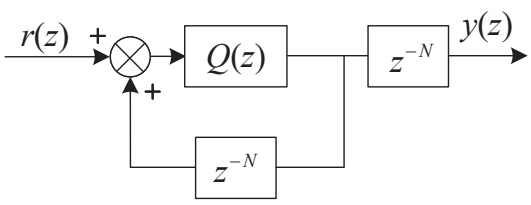

Figure 2. Block diagram of CRC.

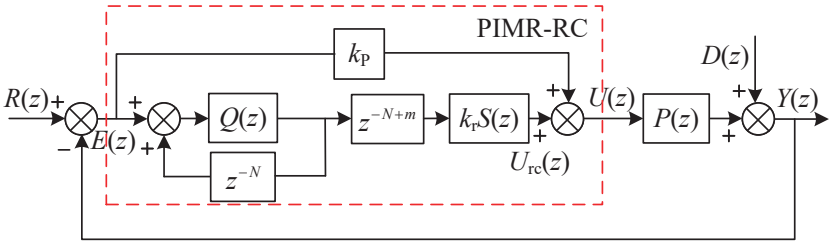

Figure 3. Block diagram of the PIMR-RC system.

In Figure 3, k_r is the CRC gain, k_p is the proportional gain, z^m is the phase-lead compensator for the system delay caused by the plant and controller. $S(z)$ is a low-pass filter that maintains system stability. $P(z)$ is the plant, and $D(z)$ is the disturbance. The transfer function from $Y(z)$ to $R(z)$ can be written as

$$\begin{aligned} G_0(z) &= \frac{\left(k_p + \frac{Q(z)z^{-N}}{1-Q(z)z^{-N}} z^m k_r S(z)\right) P(z)}{1 + \left(\left(k_p + \frac{Q(z)z^{-N}}{1-Q(z)z^{-N}} z^m k_r S(z)\right) P(z)\right)} \\ &= \frac{1 - Q(z)z^{-N}}{1 - Q(z)z^{-N}(1 + k_p P(z)) + P(z)Q(z)z^{-N} z^m k_r S(z)} \\ &= \frac{1 - Q(z)z^{-N}}{1 - Q(z)z^{-N} + Q(z)z^{-N} z^m k_r S(z) P_0(z)} \\ &\approx 1 - Q(z)z^{-N} \\ &\qquad if \quad z^m k_r S(z) P_0(z) = 1. \end{aligned} \tag{5}$$

When $z^m k_r S(z) P_0(z) = 1$, the symbol of approximate equality in the above equation is valid, which is an advantageous frequency property for the RC design. In (5), $P_0(z) = P(z)/(1 + k_p P(z))$ provides CRC with a new plant [12]. In fact, k_p can make the frequency response of $P_0(z)$ close to 0 dB, and a suitably large enough k_p can produce a larger range of k_r, which can improve the dynamic response.

3.2. The Proposed IRC

The proposed modified RC is shown in Figure 4, and the transfer function can be written as

$$\begin{aligned} G(z) &= \frac{Q(z)\left(2 - Q(z)z^{-N}\right)}{1 - Q(z)(2 - Q(z)z^{-N})z^{-N}} z^{-N} \\ &= \frac{Q_1(z)z^{-N}}{1 - Q_1(z)z^{-N}}, \end{aligned} \tag{6}$$

where $Q_1(z) = Q(z)\left(2 - Q(z)z^{-N}\right)$ is the modified internal model filter.

Figures 5 and 6 show the frequency characteristics of the modified RC and CRC, when $Q(z) = 0.99$. As can be seen, at resonant frequencies, the modified RC has a greater gain than the CRC. Compared to CRC, the modified RC provides nearly twice the gain at 50 Hz and 100 Hz. Meanwhile, the resonant bandwidth of the modified RC is wider than CRC. Therefore, the modified RC has better harmonic rejection performance and the ability to resist frequency shifts.

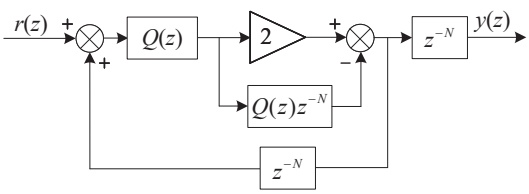

Figure 4. Block diagram of the proposed modified RC.

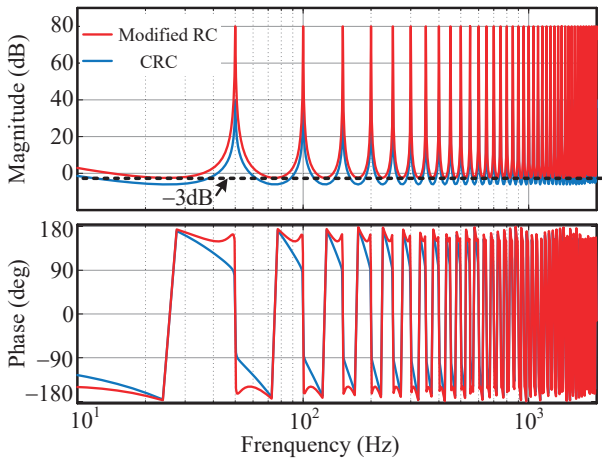

Figure 5. Bode diagram of modified RC and CRC.

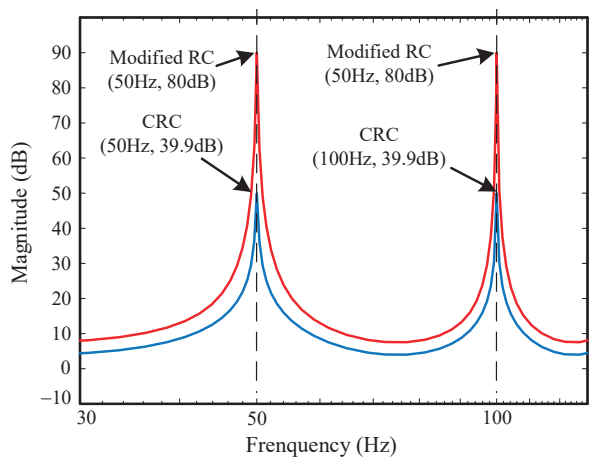

Figure 6. Magnitude response of modified RC and CRC.

In reference to the PIMR-RC, the IRC is comprised of a modified RC and a proportional controller, as shown in Figure 7. The transfer function of the system can be written as [14]

$$\begin{aligned} G_1(z) &= \frac{\left(k_p + \frac{Q_1(z)z^{-N}}{1-Q_1(z)z^{-N}} z^m k_r S(z)\right) P(z)}{1 + \left(\left(k_p + \frac{Q_1(z)z^{-N}}{1-Q_1(z)z^{-N}} z^m k_r S(z)\right) P(z)\right)} \\ &= \frac{1 - Q_1(z)z^{-N}}{1 - Q_1(z)z^{-N}\left(1 + k_p P(z)\right) + P(z)Q_1(z)z^{-N} z^m k_r S(z)} \\ &= \frac{1 - Q_1(z)z^{-N}}{1 - Q_1(z)z^{-N} + Q_1(z)z^{-N} z^m k_r S(z) P_0(z)} \\ &\approx 1 - Q_1(z)z^{-N} = G_0(z)^2 \\ &\qquad if \quad z^m k_r S(z) P_0(z) = 1, \end{aligned} \tag{7}$$

where $P_0(z) = P(z)/(1 + k_p P(z))$. By comparing (5) and (7), it is clear that G_1 is the square of the function G_0 in (5), so the amplitude of IRC with the modified $Q(z)$ filter structure, changes significantly. In fact, higher gain means a better harmonic rejection performance in this control system. However, the gain of the IRC also drops off severely when the grid fluctuates. Therefore, we need to ensure that its resonant frequency follows the grid frequency.

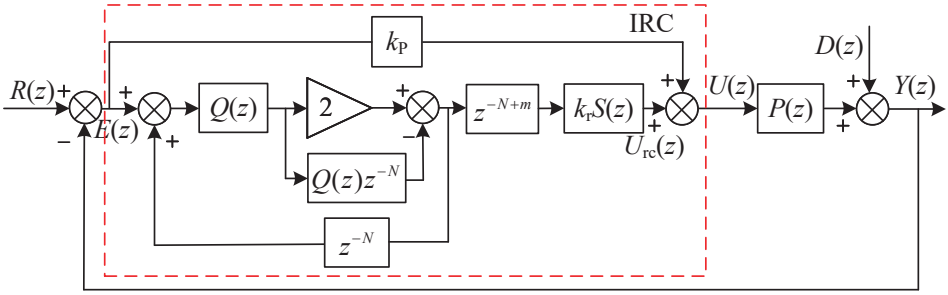

Figure 7. Block diagram of the proposed IRC system.

4. The Proposed Frequency Adaptive IRC

The grid frequency in the distributed power generation system may fluctuate [33], and $N = f_s/f_0$ may be a fraction. The values of N at different grid frequencies, when f_s = 10 kHz, are shown in Table 2.

Table 2. The corresponding RC delay, N, when the grid frequency changes.

Frequency (Hz)	49.5	49.6	49.7	49.8	49.9	50	50.1	50.2	50.3	50.4	50.5
N	202	201.6	201.2	200.8	200.4	200	199.6	199.2	198.8	198.4	198

In this case, it is possible to divide N into an integer N_i and a fraction D, as follows

$$z^{-N} = z^{-N_i} \times z^{-D}, N = N_i + D. \tag{8}$$

4.1. Fractional Delay FIR Filter

The FIR filter approximates the fractional delay, using the following expression [34]

$$z^{-D} \approx H(z) = \sum_{n=0}^{M} h(n) z^{-n}, \tag{9}$$

where M represents the filter order and $h(n)$ represents the polynomial coefficient.

The coefficient $h(n)$, can be determined by the Lagrangian interpolation method, and is calculated as follows [34]

$$h(n) = \prod_{k=0, k \neq n}^{M} \frac{D-k}{n-k}, n = 0, 1, 2, \ldots, M. \tag{10}$$

Coefficients for the Lagrange FD filter, with orders $M = 1$, 2, and 3, are given in Table 3 [35].

Table 3. Coefficients of the Lagrange FD filter.

	$\boldsymbol{M = 1}$	$\boldsymbol{M = 2}$	$\boldsymbol{M = 3}$
$h(0)$	$1 - D$	$(D-1)(D-2)/2$	$-(D-1)(D-2)(D-3)/6$
$h(1)$	D	$-D(D-2)$	$D(D-2)(D-3)/2$
$h(2)$		$D(D-1)/2$	$-D(D-1)(D-3)/2$
$h(3)$			$D(D-1)(D-2)/6$

The best interpolation is achieved, when the interpolation point D, is close to the center of the sampled data, namely $D \approx M/2$. In addition, a larger M can achieve higher accuracy, but the computational effort becomes larger. In this article, a third-order FIR filter is used. For example, when f_s = 10 kHz, if f_0 changes to 49.6 Hz, then N = 201.6, $z^{-201.6}$ can be expressed as $z^{-200}z^{-1.6}$. According to Table 3,

$$z^{-1.6} = h(0)z^0 + h(1)z^{-1} + h(2)z^{-2} + h(3)z^{-3} = -0.056 + 0.448z^{-1} + 0.672z^{-2} - 0.064z^{-3}, \tag{11}$$

and

$$z^{-201.6} = z^{-201} \times (-0.056 + 0.448z^{-1} + 0.672z^{-2} - 0.064z^{-3}). \tag{12}$$

To obtain a high accuracy, the value of D is selected to be between 1.2 and 1.8 when the grid frequency varies. The frequency responses of FD filters based on Lagrangian interpolation, are shown in Figure 8 for different fractions of D, from 1.2 to 1.8, with order M = 3. The magnitude response of the FIR filter is close to one within the passband of the FD filter, which makes it possible to design repetitive controllers without considering the effect of the FIR on the system's amplitude and frequency performance. In addition, its high frequency attenuation is more conducive to system stability. More importantly, the coefficients in the FD filter consume relatively little computational effort, so it is relatively simple to use Lagrangian interpolation to create an FD filter [36].

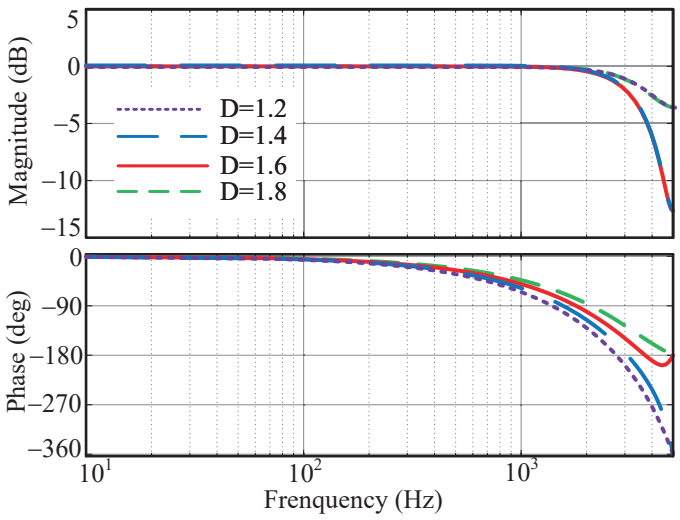

Figure 8. Frequency responses of Lagrange-interpolation-based FD filters.

4.2. Stability Analysis of FA-IRC System

The structure diagram of the FA-IRC-based inverter control system is shown in Figure 9, where $z^{-N} = z^{-N_i} \times z^{-D}$ is the delay unit of FA-IRC. z^{-D} is the fractional delay based on the FIR filter. The transfer function from i_{ref} and u_g to $E(z)$ is

$$E(z) = \frac{i_{ref}(z) - u_g(z)}{1 + G_{FO-IRC}P(z)}, \tag{13}$$

where

$$\begin{aligned} G_{FA\text{-}IRC} &= k_p + \frac{Q_1(z)z^{-N}}{1 - Q_1(z)z^{-N}} z^m k_r S(z) \\ &= k_p + G_2(z). \end{aligned} \tag{14}$$

From (13) and (14), this system has the following characteristic polynomial:

$$1 + \left[G_2(z) + k_p\right]P(z) = \left[1 + k_p P(z)\right]\left[1 + G_2(z)P_0(z)\right]. \tag{15}$$

Thus, there are two stability conditions for the FA-IRC system:

(1) The roots of $1 + k_p P(z) = 0$ within the unit circle.
(2) $1 + G_2(z)P_0(z) \neq 0$.

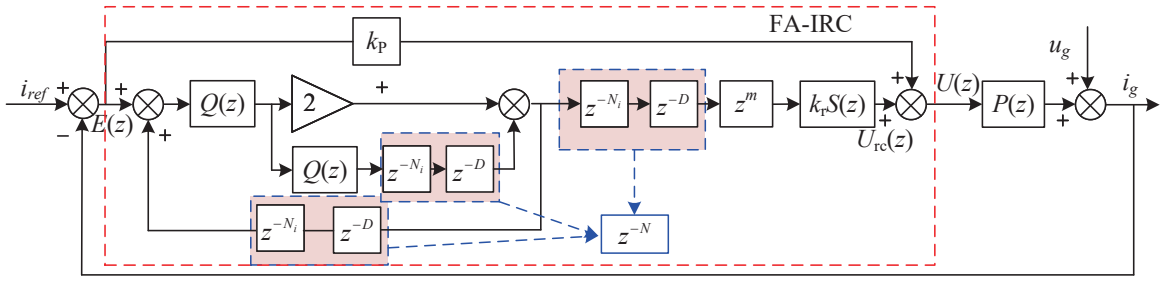

Figure 9. Block diagram of the FA-IRC system.

Obviously, the stability condition (1) is only related to the scale factor k_p, and is therefore easier to satisfy. It means that the pole of $P_0(z)$ should lie within the unit circle. Figure 10 shows the distribution of the dominant poles of $P_0(z)$ with different k_p. As can be seen, the stability condition (1) is satisfied when k_p changes from 6 to 30.

Substitute (14) into condition (2),

$$|1 - Q_1(z)z^{-N} + Q_1(z)z^{-N}z^m k_r S(z)P_0(z))| \neq 0, \quad \forall z = e^{j\omega T}, 0 < \omega < \frac{\pi}{T}, \tag{16}$$

Expression (16) can be guaranteed if [12]

$$|Q_1(z)z^{-N}(1 - z^m k_r S(z)P_0(z))| < 1, \quad \forall z = e^{j\omega T}, 0 < \omega < \frac{\pi}{T}. \tag{17}$$

If the frequency of reference signal i_{ref} and disturbance u_g approach $\omega_l = 2\pi l/N$, with $l = 0, 1, 2, \ldots, L$ ($L = N/2$ for even N and $L = (N-1)/2$ for odd N), then $z^N = 1$ [22]. Then, we have

$$|Q_1(z)(1 - z^m k_r S(z)P_0(z))| < 1, z = e^{j\omega T}. \tag{18}$$

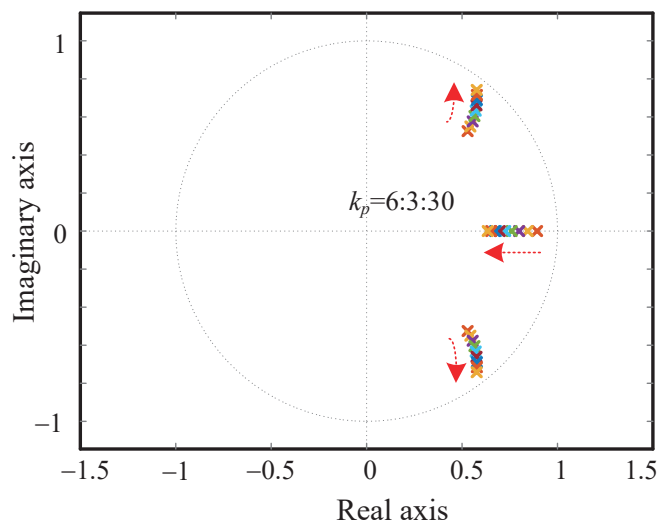

Figure 10. Distribution of the dominant poles of $P_0(z)$ with different k_p.

The Bode diagram of $Q_1(z)$ with $Q(z) = 0.99$ and $Q(z) = 0.25z + 0.5 + 0.25z^{-1}$, is shown in Figure 11. It is obvious that the magnitude characteristic of $Q_1(z)$ is greater than 0, then (18) can be written as

$$|(1 - z^m k_r S(z)P_0(z))| < \frac{1}{Q_1(z)}, z = e^{j\omega T}. \tag{19}$$

Let $N_s(\omega)$, $N_{P_0}(\omega)$, and $N_{Q_1}(\omega)$ represent the magnitude characteristics of $S(z)$, $P_0(z)$, and $Q_1(z)$, respectively, and $\theta_s(\omega)$, $\theta_{p_0}(\omega)$, and $\theta_{Q_1}(\omega)$ represent their phase characteristics. They can be written as follows

$$\begin{aligned} P_0\left(e^{j\omega T_s}\right) &= N_{P_0}\left(e^{j\omega T_s}\right)\exp\left[j\theta_{P_0}\left(e^{j\omega T_s}\right)\right], \\ S\left(e^{j\omega T_s}\right) &= N_s\left(e^{j\omega T_s}\right)\exp\left[j\theta_s\left(e^{j\omega T_s}\right)\right], \\ Q_1(z)\left(e^{j\omega T_s}\right) &= N_{Q_1}\left(e^{j\omega T_s}\right)\exp\left[j\theta_{Q_1}\left(e^{j\omega T_s}\right)\right]. \end{aligned} \tag{20}$$

Then, (20) can be written as

$$\begin{aligned} &\left|1 - k_r N_S\left(e^{j\omega}\right) N_{P_0}\left(e^{j\omega}\right) e^{-j\left[\theta_S\left(e^{j\omega}\right)+\theta_{P_0}\left(e^{j\omega}\right)+m\omega\right]}\right| \\ &\qquad < \frac{1}{N_{Q_1}\left(e^{j\omega}\right) e^{-j\theta_{Q_1}\left(e^{j\omega}\right)}}. \end{aligned} \tag{21}$$

According to Euler's formula, since $k_r > 0$, $N_s(\omega)$, $N_{P_0}(\omega)$, and $N_{Q_1}(\omega)$ are also greater than 0. In order to maintain stability, the following conditions must be met

$$\left|\theta_s(\omega) + \theta_{p_0}(\omega) + m\omega T_s - \theta_{Q_1}(\omega)\right| < 90^\circ, \tag{22}$$

$$0 < k_r < \min \frac{2\cos\left[\theta_s(\omega) + \theta_{p_0}(\omega) + m\omega T_s - \theta_{Q_1}(\omega)\right]}{N_{Q_1}(\omega) N_s(\omega) N_{p_0}(\omega)}. \tag{23}$$

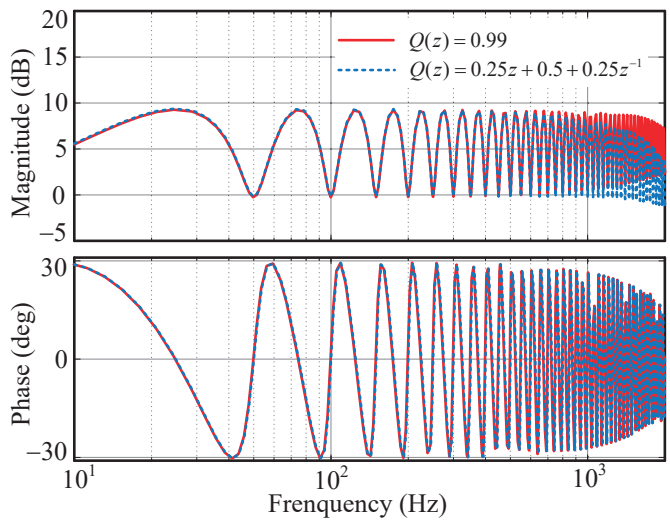

Figure 11. Bode diagram of $Q_1(z)$ with $Q(z) = 0.99$, and $Q(z) = 0.25z + 0.5 + 0.25z^{-1}$.

4.3. Characteristic Analysis

The Bode diagrams of the IRC and the FA-IRC under different N are shown in Figure 12. These show that, as the frequency increases, the deviation of the resonant frequency of the ideal IRC from the actual grid frequency and harmonic frequency, becomes larger. As a result, the reference signal tracking and harmonic rejection performance of the IRC degrades when the grid frequency fluctuates. Figure 13 describes the magnitude response around the fundamental frequency. It indicates that the amplitude of IRC is 79.8 dB at 50 Hz, whereas the amplitude of IRC decreases to 52 dB at 49.6 Hz and 50.4 Hz. While the FA-IRC's resonant frequency can follow the actual frequency of the grid, it still has a large gain at 49.6 Hz and 50.4 Hz. This means that the FA-IRC can effectively eliminate harmonics when the grid frequency varies.

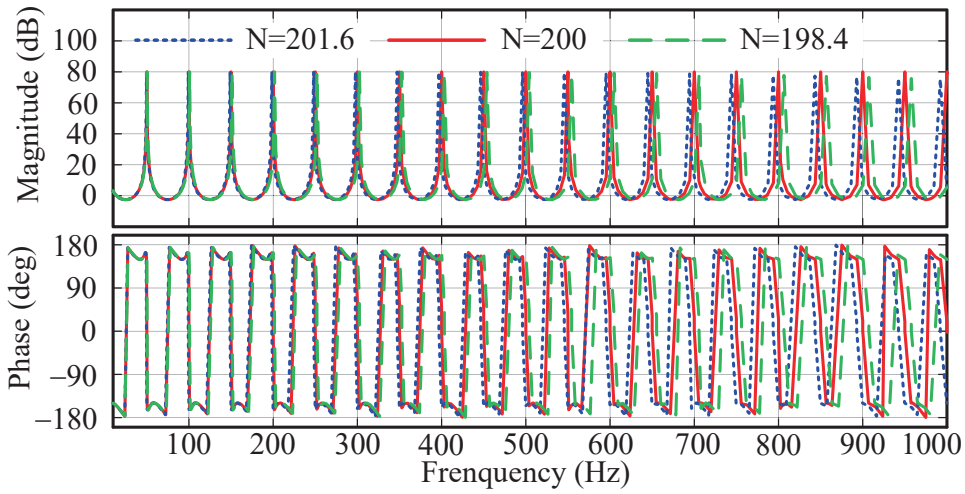

Figure 12. Bode diagrams of IRC (N = 200) and FA-IRC (N = 198.4 and 201.6).

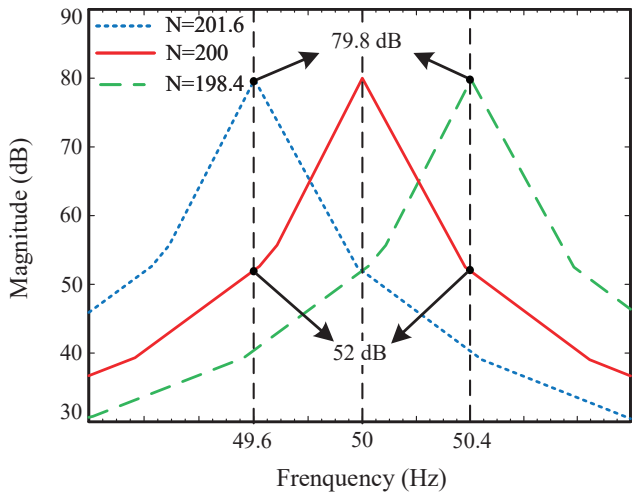

Figure 13. Magnitude characteristics of IRC (N = 200) and FA-IRC (N = 198.4 and 201.6) at the fundamental frequency.

5. Simulation Verification

In order to verify the performance of the proposed FA-IRC, a single-phase inverter control system based on this method was built using MATLAB/Simulink. The parameters of this system are shown in Table 1. According to [12] and the analysis above, the parameters of FA-IRC were selected as follows: k_p = 18, k_r = 5, m = 8, $Q(z) = 0.25z + 0.5 + 0.25z^{-1}$, and the fourth-order Butterworth low-pass filter $S(z)$, with cutoff frequency 1 kHz, is as follows

$$S(z) = \frac{0.028z^4 + 0.053z^3 + 0.071z^2 + 0.053z + 0.028}{z^4 - 2.206z^3 + 2.148z^2 - 1.159z + 0.279}. \tag{24}$$

For verifying the current tracking performance and the dynamic performance of the proposed FA-IRC, experimental results are compared with the CRC plus a proportional controller system (PIMR-RC system). In the PIMR-RC system, all control parameters remain fixed.

5.1. Steady State Response

The steady-state response is examined under a reference current of 20 A amplitude. When f_g is 50 Hz, the simulation results of the injected current i_g, and grid voltage u_g, under PIMR-RC are shown in Figure 14. The THD value of i_g is 0.60%. In addition, the THD

value of FA-IRC is 0.67% when f_g is 50 Hz, as can be obtained from Figure 15. Clearly, both control systems are effective in suppressing harmonics when f_g is 50 Hz.

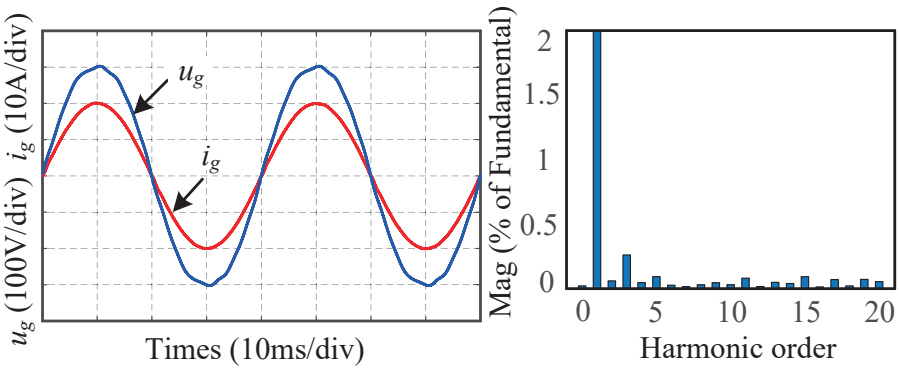

Figure 14. Output waveforms of the PIMR-RC system and spectrum analysis of the output current when f_g = 50 Hz.

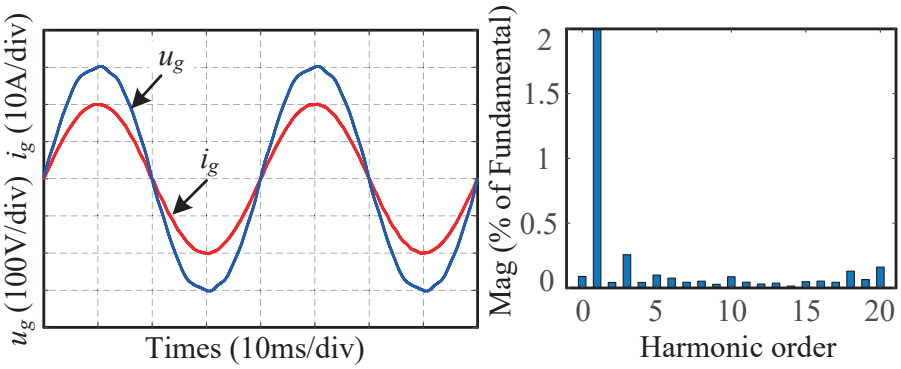

Figure 15. Output waveforms of the FA-IRC system and spectrum analysis of the output current when f_g = 50 Hz.

When f_g is set at 49.6 Hz, PIMR-RC still takes the order of RC as 200, and the THD of i_g increases to 1.70%, as shown in Figure 16. However, the THD value of i_g under FA-IRC is 0.59%, as shown in Figure 17. The reason why this is the case, is that the resonant frequencies of FA-IRC are very close to the actual grid frequency and harmonic frequencies. Figures 18 and 19 show similar results, to demonstrate the effectiveness of FA-IRC when the grid frequency is set at 50.4 Hz. The figures indicate that the THD of i_g, with FA-IRC based on the FIR filter, is 0.70%, while it is 1.73% for i_g with IRC.

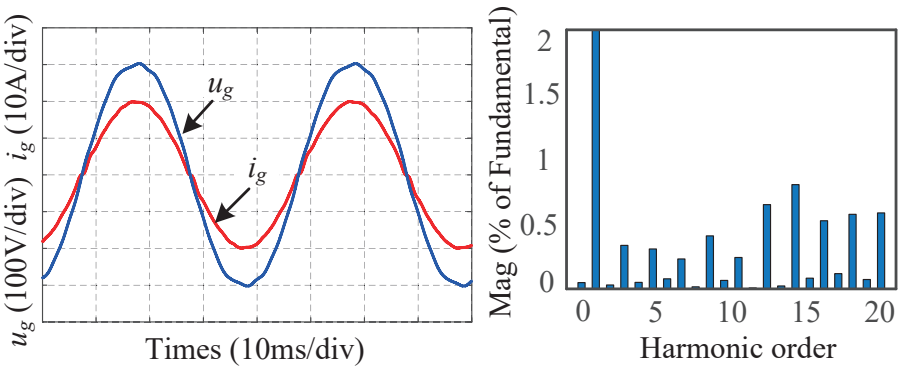

Figure 16. Output waveforms of the PIMR-RC system and spectrum analysis of the output current when f_g = 49.6 Hz.

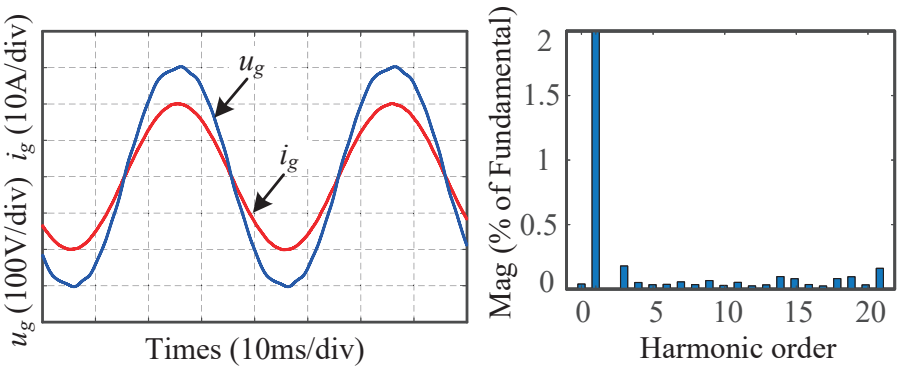

Figure 17. Output waveforms of the FA-IRC system and spectrum analysis of the output current when f_g = 49.6 Hz.

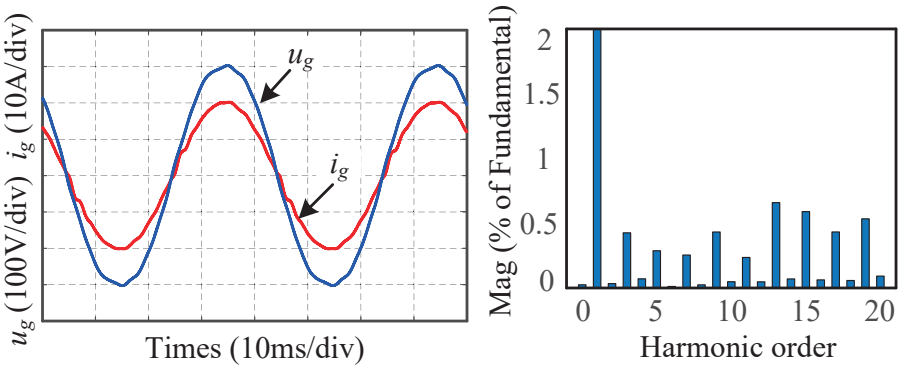

Figure 18. Output waveforms of the PIMR-RC system and spectrum analysis of the output current when f_g = 50.4 Hz.

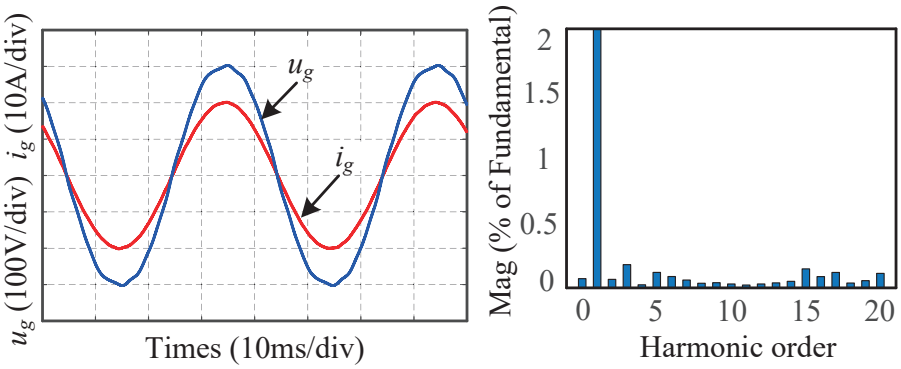

Figure 19. Output waveforms of the FA-IRC system and spectrum analysis of the output current when f_g = 50.4 Hz.

In fact, the use of Thiran-based IIR fractional delay filter during grid frequency fluctuations has been proposed in many studies of frequency adaptation [20,28]. In order to validate the frequency adaptation of the proposed scheme, a frequency adaptive IRC, based on a second-order IIR filter, has been built. In addition, to verify the harmonic rejection capability of the RC, a quasi-proportional resonant (QPR) control system is added for comparison [37]. The parameters are selected as follows: $k_p = 8$, $k_r = 4$, and $\omega_c = 5$ rad/s. The THD results of different control systems at different grid frequencies are summarized in Table 4. Table 4 indicates that the QPR control system is not affected by frequency variations, however, it has a higher THD compared to the RC based control system. In addition, it shows that the CRC and IRC systems are impacted by frequency changes to some extent. However, the proposed FA-IRC, and frequency adaptive IRC based on the IIR filter, maintain low THD values, due to their frequency adaptability.

Table 4. THD results of different control systems under various fundamental frequencies.

Fundamental Frequency (Hz)	THD Results of Different Control Systems (%)				
f_g	QPR	CRC	IRC	IRC with IIR	Proposed FA-IRC
49.6	4.19	1.70	2.36	0.62	0.59
49.7	4.19	1.52	1.51	0.67	0.66
49.8	3.97	1.22	0.99	0.72	0.59
49.9	3.96	0.80	0.75	0.67	0.68
50	3.91	0.60	0.67	0.67	0.67
50.1	3.98	0.91	0.84	0.64	0.67
50.2	3.87	1.43	1.59	0.64	0.66
50.3	3.80	1.69	2.17	0.68	0.61
50.4	3.93	1.73	2.40	0.62	0.70

5.2. Transient Response

To verify the dynamic performance of the proposed FA-IRC, the transient response of reference current amplitude changes is illustrated. Figures 20 and 21 give the transient waveforms and current error when the amplitude of i_{ref} drops from 20 A to 10 A, at different frequencies. The FA-IRC system can reach stability within 80 ms. Compared to the PIMR-RC system, the convergence rate of the FA-IRC system, with the same large gain, is equally fast. Furthermore, the current error of the FA-IRC system is approximately 0.04 A at grid frequencies of 49.6 Hz and 50.4 Hz, however, the current error of the PIMR-RC system is 0.2 A. Therefore, the proposed method can achieve good current tracking performance and dynamic performance when the grid frequency changes.

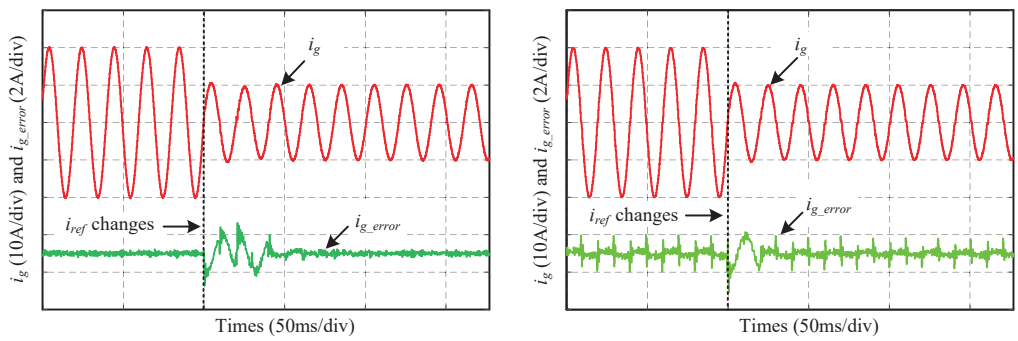

(**a**) (**b**)

Figure 20. Transient waveforms and current errors of different control systems when reference current changes, with grid frequency $f_g = 49.6$ Hz. (**a**) FA-IRC system. (**b**) PIMR-RC system.

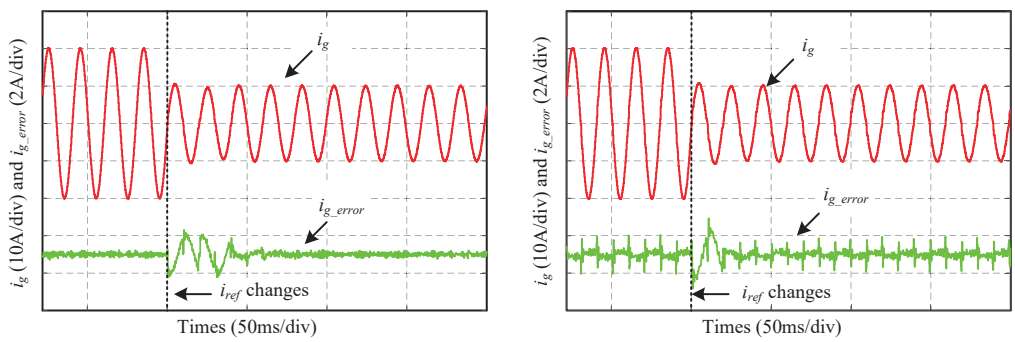

(**a**) (**b**)

Figure 21. Transient waveforms and current errors of different control systems when reference current changes, with grid frequency $f_g = 50.4$ Hz. (**a**) FA-IRC system. (**b**) PIMR-RC system.

6. Conclusions

This paper proposes an FA-IRC with a fixed sampling rate, to reject the harmonic components in the injected current of grid-tied inverters when grid frequency varies. The control strategy is based on a novel improved repetitive control. The improved repetitive control, with a modified internal model $Q(z)$ filter and a positive proportional gain, has a higher gain and bandwidth at resonant frequencies. Therefore, it has good dynamic performance. Moreover, to achieve frequency adaptive capability, a fractional-order delay, based on a polynomial Lagrange interpolating FIR filter, is built into the system. The FA-IRC system can output high quality current when the grid fundamental frequency varies within ± 0.4 Hz, because it makes the resonant frequency of the IRC approximate the actual grid frequency and harmonic frequency. Simulation results demonstrate that the FA-IRC is effective at resisting variations in grid frequency.

It is worth mentioning that, for the control methods of the grid-tied inverters considered in this paper, grid voltage magnitude fluctuations and grid impedance variations, which are common in distributed generation systems, are not taken into account. The impedance analysis method is an important tool for the stability of grid-tied inverter–grid interaction systems. It conveniently implements the modeling of the frequency characteristics of the grid-tied inverter system, and effectively simplifies the complexity of the grid-tied inverter system impedance stability analysis during grid changes. In addition, the inverter–grid system can be kept stable with reasonable grid voltage feedforward values. These cases should be considered in future work.

Author Contributions: Conceptualization, H.Z. and Q.Z.; methodology, H.Z.; investigation, H.Z., Q.Z., S.W. and X.Y.; writing—original draft preparation, H.Z.; writing—review and editing, H.Z., Q.Z., S.W. and X.Y.; supervision, H.Z. All authors have read and agreed to the published version of the manuscript.

Funding: This work was supported in part by the National Natural Science Foundation of China, under grant 61973157 and 62073297, in part by the Natural Science Foundation of Henan Province, under grant 232300421239, in part by the Science and Technology Innovation Team of Colleges and Universities in Henan Province, under grant 22IRTSTHN015, and in part by the Incubation Program for Young Master Supervisor of Zhongyuan University of Technology, under grant D202213.

Data Availability Statement: All data generated or analysed during this study are included in this published article.

Conflicts of Interest: The authors declare no conflict of interest.

Abbreviations

The following abbreviations are used in this manuscript:

IRC	Improved repetitive control
RC	Repetitive control
CRC	Conventional repetitive control
HORC	Higher-order repetitive control
FA-IRC	Frequency adaptive improved repetitive control
FD	Fractional delay
FIR	Finite impulse response
IIR	Infinite impulse response
PIMR-RC	Proportional integral multi resonant-type repetitive control
IMP	Internal model principle
THD	Total harmonic distortion
PWM	Pulse width modulation
ZOH	Zero-order holder
PLL	Phase-locked loop
PCC	Point of common coupling
QPR	Quasi-proportional resonant

References

1. Abdullah, M.A.; Muttaqi, K.M.; Agalgaonkar, A.P. Sustainable energy system design with distributed renewable resources considering economic, environmental and uncertainty aspects. *Renew. Energy* **2015**, *78*, 165–172. [CrossRef]
2. Seifi, K.; Moallem, M. Synchronization and control of a single-phase grid-tied inverter under harmonic distortion. *Electronics* **2023**, *12*, 860. [CrossRef]
3. Yang, Y.; Zhou, K.; Blaabjerg, F. Current harmonics from single-phase grid-connected inverters—Examination and suppression. *IEEE J. Emerg. Sel. Top. Power Electron.* **2015**, *4*, 221–233. [CrossRef]
4. Lunardi, A.; Conde, E.; Assis, J.; Meegahapola, L. Repetitive predictive control for current control of grid-connected inverter under distorted voltage conditions. *IEEE Access* **2022**, *10*, 16931–16941. [CrossRef]
5. Peng, F.; Xie, W.; Yan, J. State feedback and deadbeat predictive repetitive control of three-phase Z-source inverter. *Electronics* **2023**, *12*, 1005. [CrossRef]
6. Ramos, G.A.; Costa-Castelló, R. Comparison of different repetitive control architectures: Synthesis and comparison. application to VSI converters. *Electronics* **2018**, *7*, 446. [CrossRef]
7. Jiang, S.; Cao, D.; Li, Y.; Liu, J.; Peng, F.Z. Low-THD, fast-transient, and cost-effective synchronous-frame repetitive controller for three-phase UPS inverters. *IEEE Trans. Power Electron.* **2012**, *27*, 2994–3005. [CrossRef]
8. Yang, Y.; Zhou, K.; Cheng, M.; Zhang, B. Phase compensation multiresonant control of CVCF PWM converters. *IEEE Trans. Power Electron.* **2012**, *28*, 3923–3930. [CrossRef]
9. Zhao, Q.; Ye, Y. Fractional phase lead compensation RC for an inverter: Analysis, design, and verification. *IEEE Trans. Ind. Electron.* **2016**, *64*, 3127–3136. [CrossRef]
10. Chen, S.; Zhao, Q.; Ye, Y.; Qu, B. Using IIR filter in fractional order phase lead compensation PIMR-RC for grid-tied inverters. *IEEE Trans. Ind. Electron.* 2022, *in press*. [CrossRef]
11. Wang, Y.; Darwish, A.; Holliday, D.; Williams, B.W. Plug-in repetitive control strategy for high-order wide-output range impedance-source converters. *IEEE Trans. Power Electron.* **2016**, *32*, 6510–6522. [CrossRef]
12. Zhao, Q.; Ye, Y. A PIMR-type repetitive control for a grid-tied inverter: Structure, analysis, and design. *IEEE Trans. Power Electron.* **2017**, *33*, 2730–2739. [CrossRef]
13. Kim, B.S.; Tsao, T.C. Robust repetitive controller design with improved performance. In Proceedings of the 2001 American Control Conference, Arlington, VA, USA, 25–27 June 2001; pp. 2027–2032.
14. Pandove, G.; Singh, M. Robust repetitive control design for a three-phase four wire shunt active power filter. *IEEE Trans. Ind. Informat.* **2018**, *15*, 2810–2818. [CrossRef]
15. Kurniawan, E.; Cao, Z.; Man, Z. Design of robust repetitive control with time-varying sampling periods. *IEEE Trans. Ind. Electron.* **2014**, *61*, 2834–2841. [CrossRef]
16. Kolluri, S.; Gorla, N.B.Y.; Sapkota, R.; Panda, S.K. A new control architecture with spatial comb filter and spatial repetitive controller for circulating current harmonics elimination in a droop-regulated modular multilevel converter for wind farm application. *IEEE Trans. Power Electron.* **2019**, *34*, 10509–10523. [CrossRef]
17. Song, Y.; Nian, H. Sinusoidal output current implementation of DFIG using repetitive control under a generalized harmonic power grid with frequency deviation. *IEEE Trans. Power Electron.* **2015**, *30*, 6751–6762. [CrossRef]
18. Zhu, M.; Ye, Y.; Xiong, Y.; Zhao, Q. Multibandwidth repetitive control resisting frequency variation in grid-tied inverters. *IEEE J. Emerg. Sel. Top. Power Electron.* **2021**, *10*, 446–454. [CrossRef]
19. Lu, W.; Wang, W.; Zhou, K.; Fan, Q. General high-order selective harmonic repetitive control for PWM converters. *IEEE J. Emerg. Sel. Top. Power Electron.* **2022**, *10*, 1178–1191. [CrossRef]
20. Zhao, Q.; Zhang, H.; Gao, Y.; Chen, S.; Wang, Y. Novel fractional-order repetitive controller based on Thiran IIR filter for grid-connected inverters. *IEEE Access* **2022**, *10*, 82015–82024. [CrossRef]
21. Escobar, G.; Hernandez-Gomez, M.; Valdez-Fernandez, A.A.; Lopez-Sanchez, M.J.; Catzin-Contreras, G.A. Implementation of a $6n \pm 1$ repetitive controller subject to fractional delays. *IEEE Trans. Ind. Electron.* **2015**, *62*, 444–452. [CrossRef]
22. Yang, Y.; Zhou, K.; Wang, H.; Blaabjerg, F.; Wang, D.; Zhang, B. Frequency adaptive selective harmonic control for grid-connected inverters. *IEEE Trans. Power Electron.* **2015**, *30*, 3912–3924. [CrossRef]
23. Zhao, Q.; Chen, S.; Wen, S.; Qu, B.; Ye, Y. A frequency adaptive PIMR-type repetitive control for a grid-tied inverter. *IEEE Access* **2018**, *6*, 65418–65428. [CrossRef]
24. Jamil, M.; Waris, A.; Gilani, S.O.; Khawaja, B.A.; Khan, M.N.; Raza, A. Design of robust higher-order repetitive controller using phase lead compensator. *IEEE Access* **2020**, *8*, 30603–30614. [CrossRef]
25. Chen, Y.; Zhou, K.; Tang, C.; Shu, Y.; Yang, Y. Fractional-order multiperiodic odd-harmonic repetitive control of programmable AC power sources. *IEEE Trans. Power Electron.* **2022**, *37*, 7751–7758. [CrossRef]
26. Chen, D.; Zhang, J.; Qian, Z. An Improved repetitive control scheme for grid-connected inverter with frequency-adaptive capability. *IEEE Trans. Ind. Electron.* **2013**, *60*, 814–823. [CrossRef]
27. Zou, Z.X.; Zhou, K.; Wang, Z.; Cheng, M. Frequency-adaptive fractional-order repetitive control of shunt active power filters. *IEEE Trans. Ind. Electron.* **2015**, *62*, 1659–1668. [CrossRef]
28. Ye, J.; Liu, L.; Xu, J.; Shen, A. Frequency adaptive proportional-repetitive control for grid-connected inverters. *IEEE Trans. Ind. Electron.* **2021**, *68*, 7965–7974. [CrossRef]

29. Jalili, K.; Bernet, S. Design of LCL filters of active-front-end two-level voltage-source converters. *IEEE Trans. Ind. Electron.* **2009**, *56*, 1674–1689. [CrossRef]
30. Zhang, Z.; Ding, W. Improved active disturbance rejection control strategy for LCL-type grid-connected inverters based on the backstepping method. *Electronics* **2022**, *11*, 2237. [CrossRef]
31. Wang, X.; Zhuang, R.; Cai, J. Theoretical analysis of a fractional-order LLCL filter for grid-tied inverters. *Fractal Fract.* **2023**, *7*, 135. [CrossRef]
32. Cespedes, M.; Sun, J. Adaptive Control of Grid-Connected Inverters Based on Online Grid Impedance Measurements. *IEEE Trans. Sustain. Energy* **2014**, *5*, 516–523. [CrossRef]
33. *IEEE Standard 1547.2-2008*; IEEE Application Guide for IEEE Std 1547, IEEE Standard for Interconnecting Distributed Resources with Electric Power Systems. IEEE: New York, NY, USA, 2009.
34. Laakso, T.I.; Valimaki, V.; Karjalainen, M.; Laine, U.K. Splitting the unit delay [FIR/all pass filters design]. *IEEE Signal Process. Mag.* **1996**, *13*, 1996. [CrossRef]
35. Xie, C.; Zhao, X.; Savaghebi, M.; Meng, L.; Guerrero, J.M.; Vasquez, J.C. Multirate fractional-order repetitive control of shunt active power filter suitable for microgrid applications. *IEEE J. Emerg. Sel. Top. Power Electron.* **2017**, *5*, 809–819. [CrossRef]
36. Kwan, H.K.; Jiang, A. FIR, allpass, and IIR variable fractional delay digital filter design. *IEEE Trans. Circuits Syst. I Reg. Pap.* **2009**, *56*, 2064–2074. [CrossRef]
37. Zmood, D.N.; Holmes, D.G. Stationary frame current regulation of PWM inverters with zero steady-state error. *IEEE Trans. Circuits Syst. I Reg. Pap.* **2003**, *18*, 814–822. [CrossRef]